applied sciences

MDPI

Article

Controlling Refraction Using Sub-Wavelength Resonators

Yue Chen [1] and Robert Lipton [2,*]

[1] Department of Mathematics and Computer Science, Auburn University at Montgomery, Montgomery, AL 36116, USA; ychen5@aum.edu
[2] Department of Mathematics, Louisiana State University, Baton Rouge, LA 70803, USA
* Correspondence: lipton@math.lsu.edu

Received: 10 September 2018; Accepted: 11 October 2018; Published: 16 October 2018

Abstract: We construct metamaterials from sub-wavelength nonmagnetic resonators and consider the refraction of incoming signals traveling from free space into the metamaterial. We show that the direction of the transmitted signal is a function of its center frequency and bandwidth. The directionality of the transmitted signal and its frequency dependence is shown to be explicitly controlled by sub-wavelength resonances that can be calculated from the geometry of the sub-wavelength scatters. We outline how to construct a medium with both positive and negative index properties across different frequency bands in the near infrared and optical regime.

Keywords: metamaterials; refraction; signal; dispersion relation

1. Introduction

Metamaterials are patterned materials whose dispersive properties are controlled by their internal structure. The distinctive feature is that signal propagation within the metamaterial is governed by micro or nano resonators smaller than the smallest wavelength of the propagating signal. Familiar examples include stained glass and colloidal suspensions which derive their coloration from the plasmonic resonances of gold nanoparticles at optical frequencies, see [1]. Experimental validation of negative index metamaterials created using the negative effective magnetic permeability of split ring resonators [2] togeather with the negative effective dielectric constant from metal posts [3] proposed in [4] is given in the article of [5]. Refraction of Gaussian pulses by negative index slabs are theoretically investigated in [6]. Subsequent work has delivered several new designs using different configurations of metallic resonators and corrugated wave guides for double negative and effective magnetic behavior [7–20] in the microwave regime.

For higher frequencies in the infrared and optical range, new strategies for generating materials with double negative bulk properties rely on Mie resonances. One scheme employs coated rods made from a high dielectric core coated with a frequency dependent dielectric plasmonic or Drude type behavior at optical frequencies [21–23]. A second scheme employs small rods or particles made from dielectric materials with large permittivity, [24–26]. Alternate strategies for generating negative bulk dielectric permeability at infrared and optical frequencies use special configurations of plasmonic nanoparticles [27,28]. The list of metamaterial systems is growing and reviews of the subject can be found in [29,30]. Studies on random configuration of dielectric materials has been pursued recently in [31–33].

In the present work we are interested in the refraction of signals of a given center frequency and bandwidth traveling from free space into a metamaterial. We construct our metamaterial from non-magnetic sub-wavelength arrays of scatterers that exhibit both local Mie resonances as well as local plasmon resonances associated with a Drude dielectric. These resonances interlace and generate the passbands and stop bands of the metamaterial [34–37]. The resonances are shown to control the signs of the effective magnetic permeability and dielectric constant. For frequency bands where the

effective properties are simultaneously positive one has a positive dispersion while one has a negative dispersion for signals over frequency bands where effective properties are simultaneously negative, see [34–37]. The Mie resonances are generated by high dielectric fibers coated with a frequency dependent dielectric. This patterned sub-wavelength heterogeneous media delivers an effective index of refraction that can either be positive or negative across different frequency bands in the near infrared and optical regime. In this paper we outline the explicit connection linking these frequency bands to the sub-wavelength geometry and associated resonances. We illustrate the resulting positive to negative index metamaterial and the associated positive to negative angle of refraction for signals transmitted into the metamaterial over different frequency bands.

2. Metamaterials and Frequency Dependent Effective Index of Refraction

The metamaterial treated here is constructed from a two-dimensional photonic crystal made of parallel coated rods, see Figure 1. There can be one or more parallel coated rods inside the crystal period. All materials used here are nonmagnetic and have relative magnetic permeability equal to 1. We will obtain an effective magnetic response using resonant sub-wavelength geometries. The time harmonic field is TE-polarized and the magnetic field inside the crystal is parallel to the rods $\mathbf{H} = H_z(\mathbf{x}) \exp(-i\omega t)\hat{z}$ where $\mathbf{x} = (x, y)$ in the xy-plane transverse to the rods.

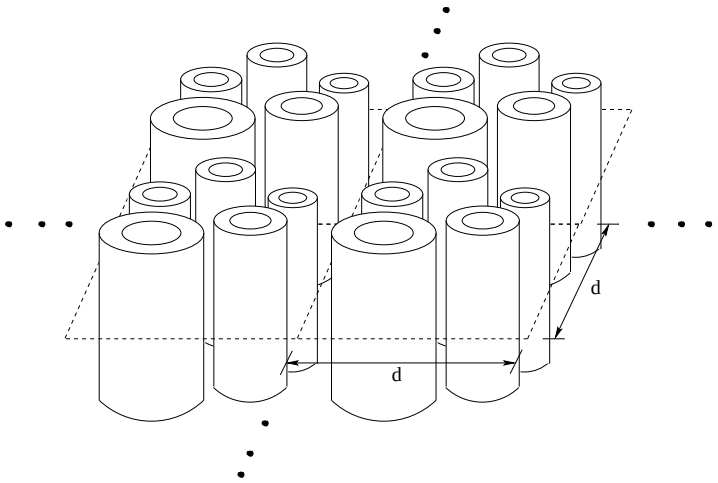

Figure 1. Photonic crystal made from coated rods.

The period for the crystal is d and the dielectric coefficient $\epsilon_d(\mathbf{x})$ takes the values

$$\epsilon_d(\mathbf{x}) = \begin{cases} \epsilon_R & \text{in the rod,} \\ \epsilon_p & \text{in the coating,} \\ \epsilon_h & \text{in the host material.} \end{cases} \tag{1}$$

The coating is a cylindrical shell of plasmonic material with dielectric constant $\epsilon_p(\omega^2/c^2) = 1 - \frac{\omega_p^2/c^2}{\omega^2/c^2}$. Here ω_p is the plasma frequency associated with the coating material and c is the speed of light in vacuum. The dielectric constant of the rod is chosen according to $\epsilon_R = \frac{\epsilon_r}{d^2}$ where ϵ_r has units of area. The idea is to choose the dielectric permittivity of the rod to be large relative to the period size so that the corresponding Mie resonances are excited in the sub-wavelength limit. The dielectric constant of the host material is given by $\epsilon_h = 1$.

The time harmonic magnetic field H_z for the d-periodic crystal is a Bloch wave

$$H_z = h(\mathbf{x}) \exp(ik_m \hat{\kappa} \cdot \mathbf{x}), \tag{2}$$

where h is d-periodic in $\mathbf{x}$, the wave number in the metamaterial is given by $k_m = 2\pi/\lambda$, where λ is the wavelength in metamaterial. The direction of propagation in the xy-plane is described by the unit vector $\hat{\kappa} = (\hat{\kappa}_x, \hat{\kappa}_y)$. The magnetic field satisfies the Helmholtz equation

$$\nabla \cdot \epsilon_d^{-1} \nabla H_z = -\frac{\omega^2}{c^2} H_z, \tag{3}$$

with propagation bands described by dispersion relations relating ω/c to $k_m\hat{\kappa}$. We examine the sub-wavelength case when $d < 2\pi c/\omega = \lambda_f$, where λ_f is the wavelength in free space. The power series approach [34,36,37] is used to find the explicit Bloch wave solution of Maxwell's equation as a convergent multiscale power series in $\eta = 2\pi d/\lambda_f$. The $\eta = 0$ term in the expansions for dispersion relation and field deliver the"homogenized sub-wavelength" dispersion relation for plane waves inside an effectively magnetic double negative medium, see [34,36,37].

In the effective medium, the dispersion relation relating frequency ω to wave number k_m is

$$k_m = \frac{\omega}{c} n_{eff}\left(\frac{\omega^2}{c^2}\right), \tag{4}$$

where n_{eff} is the effective index of refraction, and this is derived rigorously in [34].

The homogenized wave is a plane B field wave:

$$B_z^{Hom} \quad = \quad B_0 e^{i(k_m\hat{\kappa}\cdot\mathbf{x}-\omega t)},$$

where B_0 is a constant in space and time. The homogenized B field is related to the homogenized H field by $B_z^{Hom} = \mu_{eff}(\frac{\omega^2}{c^2})H_z^{Hom}$ where μ_{eff} is the effective magnetic permeability [36]. Here $H_z^{Hom} = \underline{u}_0 e^{i(k_m\hat{\kappa}\cdot\mathbf{x}-\omega t)}$ and the effective constitutive relation

$$\begin{aligned} H_z^{Hom}(\omega) &= \underline{u}_0 e^{i(k_m\hat{\kappa}\cdot\mathbf{x}-\omega t)} \\ &= \frac{B_z^{Hom}(\omega)}{\mu_{eff}(\omega)} = \frac{B_0}{\mu_{eff}(\omega)} e^{i(k_m\hat{\kappa}\cdot\mathbf{x}-\omega t)}. \end{aligned} \tag{5}$$

The effective dielectric permittivity is $\epsilon_{eff}(\frac{\omega^2}{c^2})$ and

$$n_{eff}^2 = \epsilon_{eff}\left(\frac{\omega^2}{c^2}\right)\mu_{eff}\left(\frac{\omega^2}{c^2}\right). \tag{6}$$

The explicit formulas for the frequency dependent effective magnetic permeability depend on the Dirichlet spectrum of the high contrast inclusion and the frequency dependence of the effective dielectric constant depend on the generalized electrostatic resonances (plasmon) resonances of the dielectric coating [34,36]. These formulas are presented in the next section.

3. Controlling Frequency Dependent Effective Properties and Positive and Negtive Dispersion

The frequency dependent effective magnetic permeability μ_{eff} and effective dielectric permittivity ϵ_{eff} are determined explicitly in terms of local resonances. We first rescale to a unit period cell to define effective properties. The unit cell is $Y = \{0 < x < 1; 0 < y < 1\}$. The subset of Y containing the high contrast dielectric is R, the coating containing the Drude dielectric is P and the host material occupies H. These three regions make up the unit cell Y, see Figure 2.

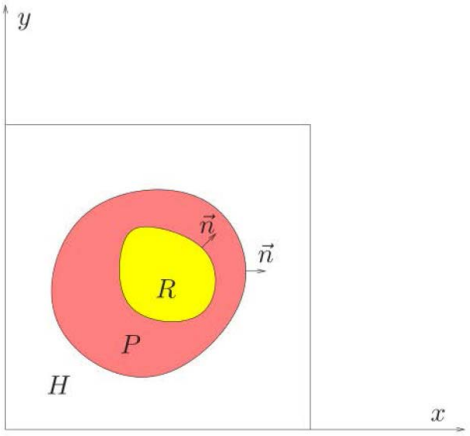

Figure 2. Unit cell containing a single rod cross section. R represents the rod cross section , P the plasmonic coating and H the host.

The Dirichlet eigenfunctions ϕ, μ

$$\begin{aligned} -\Delta\phi(\mathbf{x}) &= \mu\phi(\mathbf{x}),\ \mathbf{x} \text{ in } R \\ \phi(\mathbf{x}) &= 0,\ \mathbf{x} \text{ on the boundary of } R \end{aligned} \tag{7}$$

with nonzero mean and associated eigenvalues of the Laplacian defined on R. The set of eigen functions and eigenvalues are denoted by ϕ_n and μ_n respectively for $n = 1, 2, \cdots$. The effective magnetic permeability is given by

$$\mu_{eff}\left(\frac{\omega^2}{c^2}\right) = \theta_H + \theta_P + \sum_{n=1}^{\infty} \frac{\mu_n < \phi_n >_R^2}{\mu_n - \frac{\omega^2}{c^2}}, \tag{8}$$

where $\langle\cdot\rangle$ denotes the average over R, θ_H and θ_P are the areas occupied by regions H and P, respectively.

The generalized electrostatic resonance of the coating is the eigenfunction ψ eigenvalue γ pair solving

$$\begin{cases} \Delta\psi_{=}0 & \text{in } H, \\ \Delta\psi = 0 & \text{in } P, \end{cases} \tag{9}$$

with the boundary and transmission conditions

$$\begin{cases} \psi|^- = \psi|^+ & \text{on the boundary of } P, \\ \partial_{\vec{n}}\psi = 0 & \text{on the boundry of } R, \\ \gamma[\partial_{\vec{n}}\psi]_+^- = -\frac{1}{2}(\partial_{\vec{n}}\psi|^- + \partial_{\vec{n}}\psi|^+) & \text{on the boundary of } P, \\ \psi \text{ is } Y\text{-periodic.} \end{cases} \tag{10}$$

Here $\partial_{\vec{n}}$ is the outward directed normal derivative. The generalized electrostatic eigenvalues $\{\gamma_h\}_{h=0}^{\infty}$ lie in the open interval $(-\frac{1}{2}, \frac{1}{2})$ with zero being the only accumulation point, see [34]. The eigenfunctions $\{\psi_{\gamma_h}\}_{h=0}^{\infty}$ form a complete orthonormal set of functions in the space of mean zero square integrable periodic functions on the set $Y \setminus R$. Similar types of electrostatic resonances are well known in the context of effective coefficients of DC two phase media [38,39].

We form the integrals

$$\alpha_{\gamma_h}^1 = \int_H \nabla\psi_{\gamma_h}\, d\mathbf{x} \text{ and } \alpha_{\gamma_h}^2 = \int_P \nabla\psi_{\gamma_h}\, d\mathbf{x}. \tag{11}$$

and the frequency dependent effective dielectric constant is

$$\epsilon_{eff}^{-1}\left(\frac{\omega^2}{c^2}\right) = \theta_H + \frac{\xi_0}{\frac{\omega^2}{c^2} - \frac{\epsilon_r\omega_p^2}{c^2}}\theta_P \tag{12}$$
$$-\frac{1}{2}\sum_{-\frac{1}{2}<\gamma_h<\frac{1}{2}}\left(\frac{\left(\frac{\omega^2}{c^2} - \frac{\epsilon_r\omega_p^2}{c^2}\right)|\alpha_{\gamma_h}^{(1)}|^2 + 2\frac{\epsilon_r\omega_p^2}{c^2}\alpha_{\gamma_h}^{(1)}\cdot\alpha_{\gamma_h}^{(2)} + \frac{\left(\frac{\epsilon_r\omega_p^2}{c^2}\right)^2}{\frac{\omega^2}{c^2}-\frac{\epsilon_r\omega_p^2}{c^2}}|\alpha_{\gamma_h}^{(2)}|^2}{\frac{\omega^2}{c^2} - (\gamma_h+\frac{1}{2})\frac{\epsilon_r\omega_p^2}{c^2}}\right).$$

The index of refraction for the metamaterial is given by (6), and the dispersion relation (4). Here the the link between dispersion relation and the subwavelength geometry is explicitly given in terms of the local resonances defining the effective properties through the Formulas (8) and (12). These formulas are derived in [36,37]. It is clear that we can control the frequency dependence of μ_{eff} and ϵ_{eff} by controlling the poles and zeroes of these functions which depend on the Dirichlet resonances (7) and generalized electrostatic resonances (10) respectively. The graphs of μ_{eff} and ϵ_{eff}^{-1} as functions of ω^2/c^2 are displayed in Figures 3 and 4. Here the intervals $a' < \omega^2/c^2 < b'$ and $a'' < \omega^2/c^2 < b''$ are the same in all graphs.

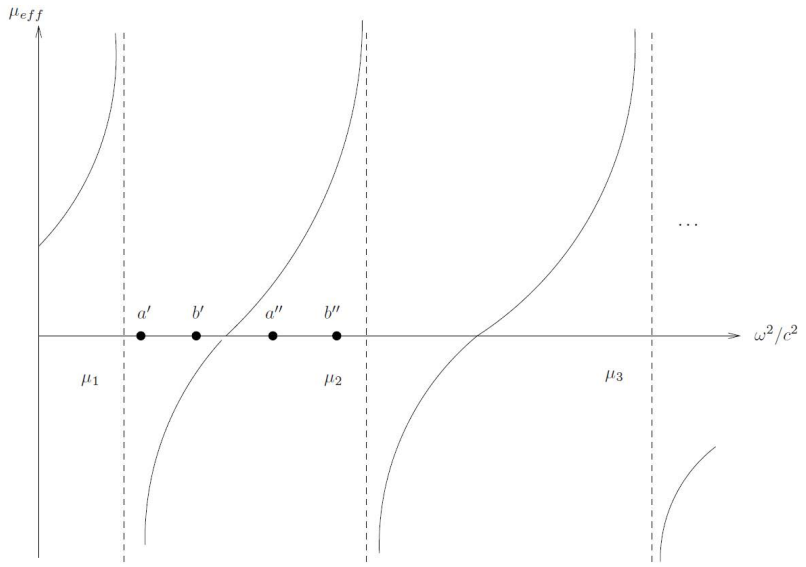

Figure 3. The relation between μ_{eff} and ω^2/c^2.

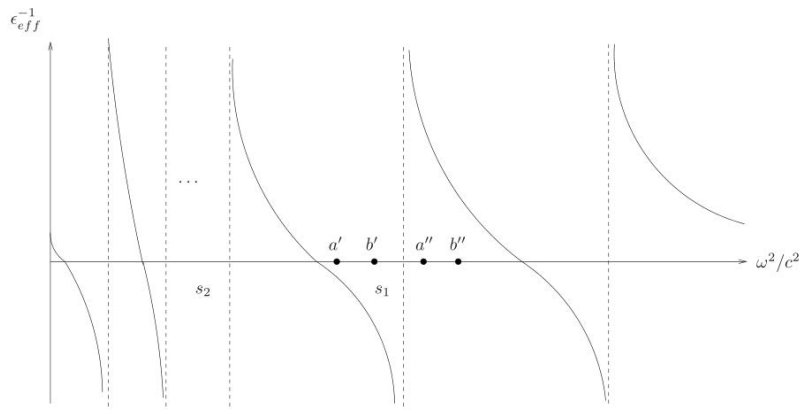

Figure 4. The relation between ϵ_{eff}^{-1} and ω^2/c^2.

It follows that dispersion relation is also controlled by the poles and zeros of μ_{eff} and ϵ_{eff}^{-1} as explicitly determined through the Dirichlet spectra and generalized electrostatic resonances. The Formulas (4) and (6) show that the frequency intervals associated with pass bands and stop bands are governed by the poles and zeros of the effective magnetic permittivity and dielectric permittivity tensors. Pass bands of fixed center frequency and band width occur when the effective magnetic permittivity and dielectric permeability have the same sign. This includes frequency intervals where effective tensors are either simultaneously positive or negative. When both are positive one has positive dispersion and negative dispersion when both are negative. Bands of positive and negative dispersion are separated by stop bands, see Figure 5.

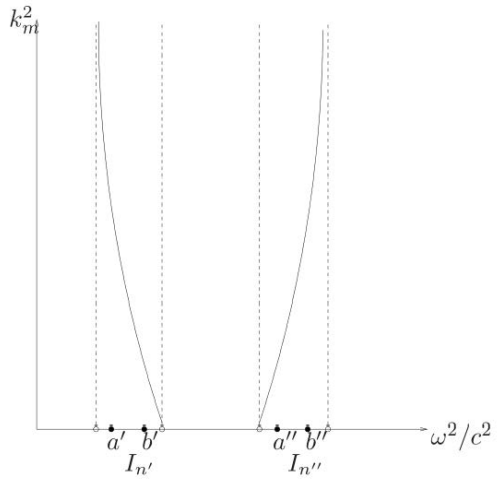

Figure 5. The leading order dispersion relation over two selected intervals $I_{n'}$ and $I_{n''}$.

In the following sections we will choose the the high contrast core phase to be a disk centered in the period cell surrounded by an annular coating of Drude dielectric. The ratios of the disk radius and the outer diameter of the coating to the period length are fixed. We then calculate the Dirichlet and electrostatic eigenvalues to calculate a frequency dependent effective index of refraction. For the concentric Drude dielectric coating-high dielectric core geometries we can control the spectra by changing the ratio of core to coating material used, see Figure 6. Here we denote the core radius by a and the outer radius of the coating by b where these numbers are in dimensionless units relative to period length. In this context we can change the outer radius of the coating and radius of the core relative to the period size. The band width and center frequency of the negative index band and its dependence on a and b listed in Table 1. This demonstrates that we can control the frequency bands where the effective index of refraction is negative (or positive) by changing the inner and outer radii of the coating material.

Table 1. The changes of the negative index band when inner radius and outer radius vary. In each cell, the upper and lower numbers denote the band width and center frequency, respectively.

	$a = 0.5b$	$a = 0.55b$	$a = 0.6b$	$a = 0.65b$
$b = 0.3$	0	0	0	0.0332 (0.8919)
$b = 0.35$	0	0.02733 (0.9003)	0.03824 (0.8315)	0.04425 (0.7716)
$b = 0.4$	0.03541 (0.8707)	0.04204 (0.7960)	0.04893 (0.7345)	0.05579 (0.6830)
$b = 0.45$	0.04366 (0.7795)	0.05143 (0.7141)	0.05944 (0.6605)	0.06801 (0.6161)

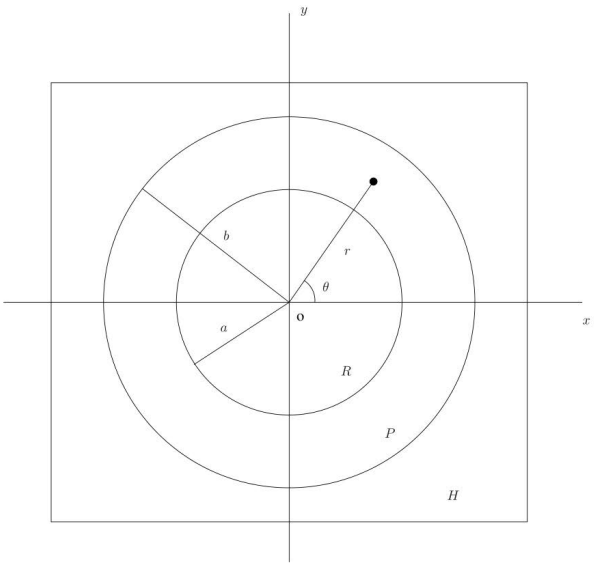

Figure 6. The crosssection of the coated fiber with core radius a and coating radius b.

These calculations highlight the frequency dependent refraction of signals composed of waves with frequencies inside different frequency bands by a free space - metamaterial system. In the following sections we demonstrate how to calculate the explicit refraction of signals passing between a free space - metamaterial interface in the time domain. We show that the same metamaterial can refract signals both positively or negatively depending only on the frequency band of the incoming signal.

In the following sections we will choose the the high contrast core phase to be a disk centered in the period cell and an annular coating. The ratios of the disk radius and the outer diameter of the coating to the period length are fixed. We then calculate Dirichlet and electrostatic eigenvalues to calculate a frequency dependent effective index of refraction. These calculations are used to highlight the frequency dependent refraction of signals composed of waves with frequencies inside different frequency bands by a free space - metamaterial system.

4. Normal Incidence on a Half Space of Metamaterial

We consider the left half space to be free space and the right half space filled with metamaterial. The interface between half spaces is parallel to the $\hat{z}$ axis and the normal to the interface is taken to be the $\hat{x}$ axis and the interface between half spaces is given by the $x = 0$ plane. We first suppose a group of waves of different frequencies propagate along the $\hat{x}$-axis, and so the H field is along the $\hat{z}$-axis and the problem reduces to one dimension.

First we consider waves inside the metamaterial. Since we have normal incidence we replace $k_m\hat{\kappa}$ by k_m and $\mathbf{x}$ by x. We let $k = \frac{\omega}{c}$ and write

$$H^{Hom}(k) \quad = \quad \frac{B^{Hom}(k)}{\mu_{eff}(ck)} = \frac{B_0}{\mu_{eff}(ck)} e^{i(k_m(k)x - kct)},$$

Energy propagation is in the direction of increasing x so if $\mu_{eff} > 0$, $\epsilon_{eff} > 0$ then $n_{eff} > 0$ while if $\mu_{eff} < 0$, $\epsilon_{eff} < 0$ then $n_{eff} < 0$, see [36,37]. On the other hand the vacuum is nonmagnetic, i.e., $\mu = 1$ so the B and H fields are the same and

$$H^{vac}(k) = B_0 e^{i(kx - kct)}, \tag{13}$$

where k is the wave number in vacuum and the free space dispersion relation is $k = \frac{\omega}{c}$.

The wave forms inside both media are a superposition of plane waves. For each k the plane waves are of the form $B_0[e^{i(kx-kct)} - \mathcal{R}(ck)e^{i(-kx-kct)}]$ for $x < 0$ and $\mathcal{T}(ck)\frac{B_0}{\mu_{eff}(ck)}e^{i(k_m(k)x-kct)}$ for $x > 0$. For each k the coefficients $\mathcal{R}(ck)$ and $\mathcal{T}(ck)$ are determined by the two transmission conditions

$$[H_3] = 0 \text{ at } x = 0 \tag{14}$$

and

$$[E_2] = 0 \text{ at } x = 0. \tag{15}$$

From Maxwell's equations we have the identity inside vacuum and metamaterial

$$E_2 = \epsilon^{-1}(x)\partial_x H_3 \tag{16}$$

where

$$\epsilon(x) = \begin{cases} 1 & \text{for } x < 0, \\ \epsilon_{eff}(ck) & \text{for } x > 0. \end{cases}$$

Then the last jump condition (15) is equivalent to

$$[\epsilon^{-1}(x)\partial_x H_3] = 0 \text{ at } x = 0. \tag{17}$$

Collecting the results we give the waveforms incident reflected and transmitted across the interface $x = 0$ between vacuum $x < 0$ and effective material $x > 0$.

Proposition 1. Waveforms in vacuum and effective material. *The $\hat{z}$ component of the H field is the only non zero component of the H field wave form in vacuum ($x < 0$) and is*

$$H_{vac}(k_0, x, t) \quad = \quad \int_{-\infty}^{\infty} A(k)B_0[e^{i(kx-kct)} - \mathcal{R}(ck)e^{i(-kx-kct)}]\, dk, \tag{18}$$

where the amplitude $A(k)$ decribes the properties of the linear superpostion of the different waves. The $\hat{z}$ component of the H field is the only nonzero component of the H field wave form in the metamaterial $(x > 0)$ and is

$$H_{eff}(k_0, x, t) \quad = \quad \int_{-\infty}^{\infty} A(k)\mathcal{T}(ck)\frac{B_0}{\mu_{eff}(ck)}e^{i(k_m(k)x-kct)}\, dk. \tag{19}$$

- *Here $H_{vac}(k_0, x, t) = H_{eff}(k_0, x, t)$ at the interface $x = 0$*

The $\hat{y}$ component of the E field is the only nonzero component of the E field in vacuum $(x < 0)$ and is

$$E_{vac}(k_0, x, t) \quad = \quad \int_{-\infty}^{\infty} A(k)B_0\frac{d}{dx}[e^{i(kx-kct)} - \mathcal{R}(ck)e^{i(-kx-kct)}]\, dk. \tag{20}$$

The $\hat{y}$ component of the E field is the only nonzero component of the E field in the metamaterial $(x > 0)$ and is

$$E_{eff}(k_0, x, t) \quad = \quad \int_{-\infty}^{\infty} A(k)\epsilon_{eff}(ck)\mathcal{T}(ck)\frac{B_0}{\mu_{eff}(ck)}\frac{d}{dx}[e^{i(k_m(k)x-kct)}]\, dk.$$

- *Here $E_{vac}(k_0, x, t) = E_{eff}(k_0, x, t)$ at the interface $x = 0$*

where

$$\mathcal{R}(ck) = \frac{1 - \epsilon_{eff}(ck)\frac{k}{k_m(ck)}}{1 + \epsilon_{eff}(ck)\frac{k}{k_m(ck)}} \tag{21}$$

and

$$\mathcal{T}(ck) = \frac{2\mu_{eff}(ck)\epsilon_{eff}(ck)}{\frac{k_m(ck)}{k} + \epsilon_{eff}(ck)}$$

Now we introduce $n^2_{eff}(ck) = \epsilon_{eff}(ck)\mu_{eff}(ck)$ and $k_m/k = n_{eff}(ck)$ and we can write

$$\mathcal{R}(ck) = \frac{1 - \frac{\epsilon_{eff}(ck)}{n_{eff}(ck)}}{1 + \frac{\epsilon_{eff}(ck)}{n_{eff}(ck)}} \tag{22}$$

and

$$\mathcal{T}(ck) = \frac{2n^2_{eff}(ck)}{1 + \frac{\epsilon_{eff}(ck)}{n_{eff}(ck)}}$$

Note that $\mathcal{R}(ck) < 1$ if $n_{eff} < 0$ and $\epsilon_{eff} < 0$.

In our paper, we consider a signal made of a group of waves with frequencies lying inside a prescribed band of frequencies for which

$$A(k) = \frac{a}{\sqrt{2\pi}} e^{-\frac{(k-k_0)^2 a^2}{2}} \hat{\chi}(\omega) \tag{23}$$

where

$$\hat{\chi}(\omega) = \begin{cases} 1 & \text{for } \omega_L \leq \omega \leq \omega_U, \\ 0 & \text{otherwise .} \end{cases}$$

In order to make the H-field dimensionless, we can use $\omega_p t$ to denote the time change, and $\frac{\omega_p x}{c}$ the position change. Let $\bar{\omega} = k_0 c$ be the center frequency. Then the transmitted wave packet (19) can be written as

$$\begin{aligned} H_{eff} &= \frac{\omega_p a}{c}\frac{1}{\sqrt{2\pi}}\int_{-\infty}^{\infty} e^{-\frac{(\frac{kc}{\omega_p}-\frac{k_0 c}{\omega_p})^2(\frac{\omega_p a}{c})^2}{2}} \hat{\chi}(\omega/\omega_p)\mathcal{T}(\omega/\omega_p)\frac{B_0}{\mu_{eff}(\omega/\omega_p)} e^{i(\frac{k_m c}{\omega_p}\frac{\omega_p x}{c} - \frac{kc}{\omega_p}(\omega_p t))}\, d(\tfrac{kc}{\omega_p}) \\ &= \frac{\omega_p a}{c}\frac{1}{\sqrt{2\pi}}\int_{-\infty}^{\infty} e^{-\frac{(\frac{\omega}{\omega_p}-\frac{\bar{\omega}}{\omega_p})^2(\frac{\omega_p a}{c})^2}{2}} \hat{\chi}(\omega/\omega_p)\mathcal{T}(\omega/\omega_p)\frac{B_0}{\mu_{eff}(\omega/\omega_p)} e^{i[(n_{eff}\frac{\omega}{\omega_p})(\frac{\omega_p x}{c}) - (\frac{\omega}{\omega_p})(\omega_p t)]}\, d(\tfrac{\omega}{\omega_p}) \end{aligned} \tag{24}$$

Similarly the reflected wave packet is

$$\begin{aligned} H_{vac} &= \frac{\omega_p a}{c}\frac{1}{\sqrt{2\pi}}\int_{-\infty}^{\infty} e^{-\frac{(\frac{\omega}{\omega_p}-\frac{\bar{\omega}}{\omega_p})^2(\frac{\omega_p a}{c})^2}{2}} \hat{\chi}(\omega/\omega_p)\times \\ & B_0[e^{i[(\frac{\omega}{\omega_p})(\frac{\omega_p x}{c}) - (\frac{\omega}{\omega_p})(\omega_p t)]} - \mathcal{R}(\omega/\omega_p) e^{i[-(\frac{\omega}{\omega_p})(\frac{\omega_p x}{c}) - (\frac{\omega}{\omega_p})(\omega_p t)]}]\, d(\tfrac{\omega}{\omega_p}). \end{aligned} \tag{25}$$

The incident wave packet without reflection is

$$\begin{aligned} H_{inc} &= \frac{a}{\sqrt{2\pi}} \int_{-\infty}^{\infty} e^{-\frac{(k-k_0)^2 a^2}{2}} \hat{\chi}(\omega) B_0 e^{i(kx-kct)}\, dk \\ &= \frac{\omega_p a}{c} \frac{1}{\sqrt{2\pi}} \int_{-\infty}^{\infty} e^{-\frac{(\frac{\omega}{\omega_p}-\frac{\bar{\omega}}{\omega_p})^2 (\frac{\omega_p a}{c})^2}{2}} \hat{\chi}(\omega/\omega_p) B_0 e^{i[(\frac{\omega}{\omega_p})(\frac{\omega_p x}{c})-(\frac{\omega}{\omega_p})(\omega_p t)]} \end{aligned} \tag{26}$$

In our example, we take $\frac{\omega_p a}{c} = 300$, $\omega_L/\omega_p = 0.735$ and $\omega_U/\omega_p = 0.74$. Let the dimensionless center frequency $\frac{\bar{\omega}}{\omega_p} = 0.7375$. We use Riemann sum to approximate the integral by the sum of two rectangles.

Let $J(\omega/\omega_p) = e^{-\frac{(\frac{\omega}{\omega_p}-\frac{\bar{\omega}}{\omega_p})^2 (\frac{\omega_p a}{c})^2}{2}} e^{i[(\frac{\omega}{\omega_p})(\frac{\omega_p x}{c})-(\frac{\omega}{\omega_p})(\omega_p t)]}$. The incident wave packet without any reflections is

$$\begin{aligned} H_{inc} &= \frac{\omega_p a}{c} \frac{1}{\sqrt{2\pi}} \int_{-\infty}^{\infty} \hat{\chi}(\omega/\omega_p) B_0 J(\omega/\omega_p)\, d(\frac{\omega}{\omega_p}) \\ &= \frac{\omega_p a}{c} \frac{1}{\sqrt{2\pi}} \int_{0.735}^{0.74} B_0 J(\omega/\omega_p)\, d(\frac{\omega}{\omega_p}) \\ &\approx \frac{\omega_p a}{c} \frac{1}{\sqrt{2\pi}} \Delta(\frac{\omega}{\omega_p}) B_0 [J(0.735) + J(0.74)], \end{aligned} \tag{27}$$

where $\frac{\omega_p a}{c} \frac{1}{\sqrt{2\pi}} \Delta(\frac{\omega}{\omega_p}) B_0$ is a constant. Figure 7 is the graph for $J(0.735) + J(0.74)$ for $\omega_p t = 5$.

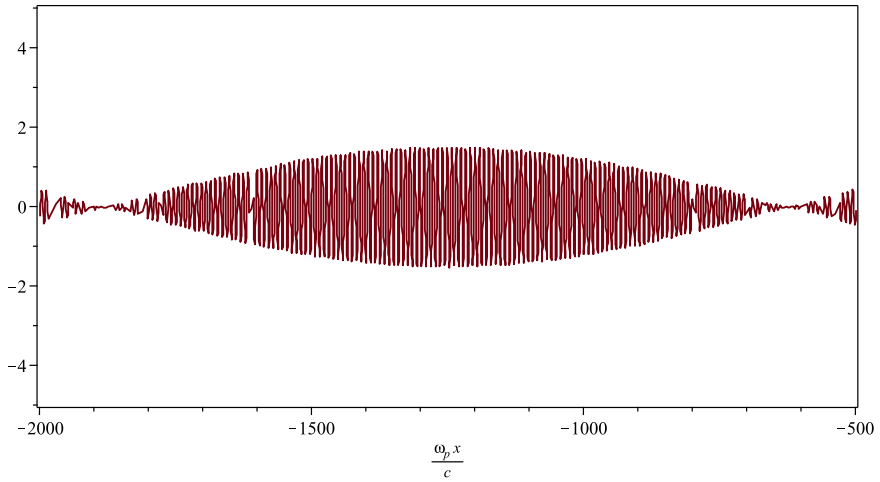

Figure 7. Incident wave without any reflection for $\omega_p t = 5$.

Let $G(\omega/\omega_p) = e^{-\frac{(\frac{\omega}{\omega_p}-\frac{\bar{\omega}}{\omega_p})^2 (\frac{\omega_p a}{c})^2}{2}} [e^{i[(\frac{\omega}{\omega_p})(\frac{\omega_p x}{c})-(\frac{\omega}{\omega_p})(\omega_p t)]} - \mathcal{R}(\omega/\omega_p) e^{i[-(\frac{\omega}{\omega_p})(\frac{\omega_p x}{c})-(\frac{\omega}{\omega_p})(\omega_p t)]}]$. The incident wave packet with the interaction of reflection is

$$\begin{aligned} H_{vac} &= \frac{\omega_p a}{c} \frac{1}{\sqrt{2\pi}} \int_{-\infty}^{\infty} \hat{\chi}(\omega/\omega_p) B_0 G(\omega/\omega_p)\, d(\frac{\omega}{\omega_p}) \\ &= \frac{\omega_p a}{c} \frac{1}{\sqrt{2\pi}} \int_{0.735}^{0.74} B_0 G(\omega/\omega_p)\, d(\frac{\omega}{\omega_p}) \\ &\approx \frac{\omega_p a}{c} \frac{1}{\sqrt{2\pi}} \Delta(\frac{\omega}{\omega_p}) B_0 [G(0.735) + G(0.74)]. \end{aligned} \tag{28}$$

Figure 8 is the graph for $G(0.735) + G(0.74)$ for $\omega_p t = 5$ which is H field in vacuum with interaction between incident and reflective waves.

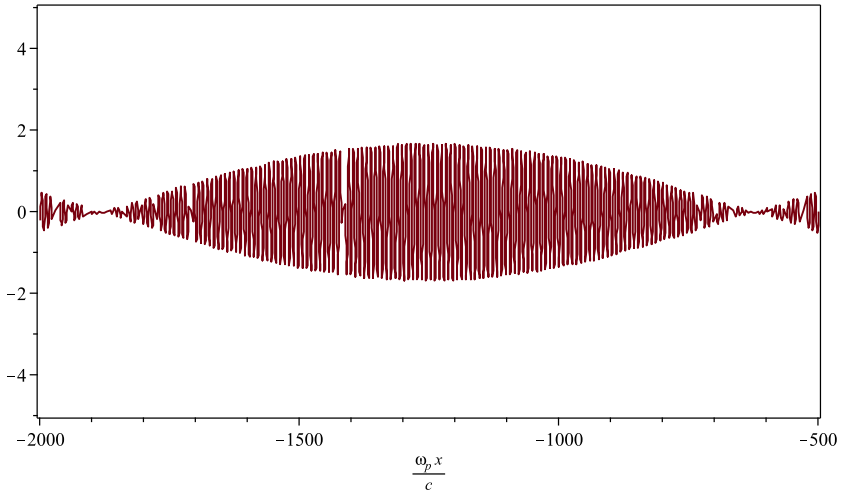

Figure 8. H field in vacuum with interaction between incident and reflective waves for $\omega_p t = 5$.

Let $F(\omega/\omega_p) = e^{-\frac{(\frac{\omega}{\omega_p}-\frac{\bar{\omega}}{\omega_p})^2(\frac{\omega_p a}{c})^2}{2}} \frac{\mathcal{T}(\omega/\omega_p)}{\mu_{eff}(\omega/\omega_p)} e^{i[(n_{eff}\frac{\omega}{\omega_p})(\frac{\omega_p x}{c})-(\frac{\omega}{\omega_p})(\omega_p t)]}$. Then we have

$$\begin{aligned} H_{eff} &= \frac{\omega_p a}{c}\frac{1}{\sqrt{2\pi}}\int_{-\infty}^{\infty}\hat{\chi}(\omega/\omega_p)B_0F(\omega/\omega_p)\,d(\frac{\omega}{\omega_p}) \\ &= \frac{\omega_p a}{c}\frac{1}{\sqrt{2\pi}}\int_{0.735}^{0.74}B_0F(\omega/\omega_p)\,d(\frac{\omega}{\omega_p}) \\ &\approx \frac{\omega_p a}{c}\frac{1}{\sqrt{2\pi}}\Delta(\frac{\omega}{\omega_p})B_0[F(0.735)+F(0.74)], \end{aligned} \tag{29}$$

where $\frac{\omega_p a}{c}\frac{1}{\sqrt{2\pi}}\Delta(\frac{\omega}{\omega_p})B_0$ is a constant. Figures 9 and 10 are the graphs for $F(0.735)+F(0.74)$ for different $\omega_p t$, i.e., the transmitted wave motion in metamaterial ($x > 0$). Figure 9 shows transmitted wave motion from the bottom to the top for $\omega_p t$ ranging from 5 to 9 in the steps of 2. It can be observed that the group velocity of the transmitted wave in metamaterial has the forward direction (the envelope moves forward). Figure 10 shows the transmitted wave motion from the bottom to the top for $\omega_p t$ ranging from 5 to 7 in the steps of 1. We can see that the phase of the transmitted wave in metamaterial moves backward.

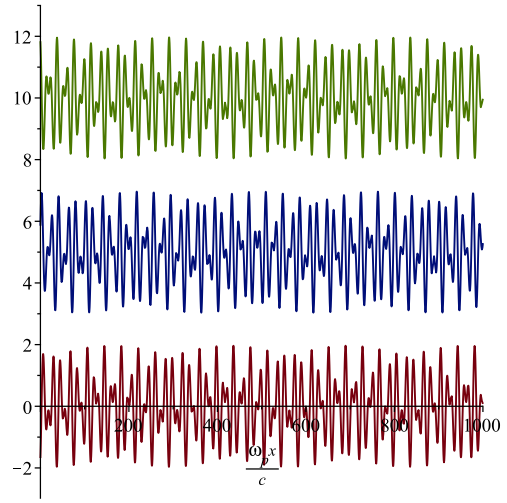

Figure 9. Transmitted wave motion from the bottom to the top for $\omega_p t$ ranging from 5 to 9 in the steps of 2. The group velocity has the forward direction.

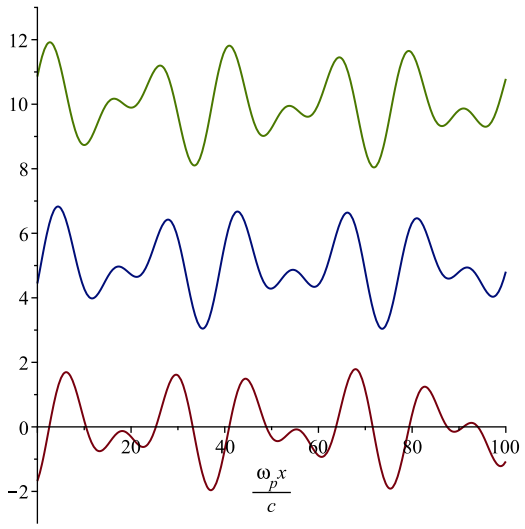

Figure 10. Transmitted wave motion from the bottom to the top for $\omega_p t$ ranging from 5 to 7 in the steps of 1. The phase velocity has the backward direction.

The H field at the interface between the vacuum ($x < 0$) and effective double negative material ($x > 0$) is shown in Figure 11. The graph shows the continuity of the magnetic field at the interface. But it is not differentiable at the interface.

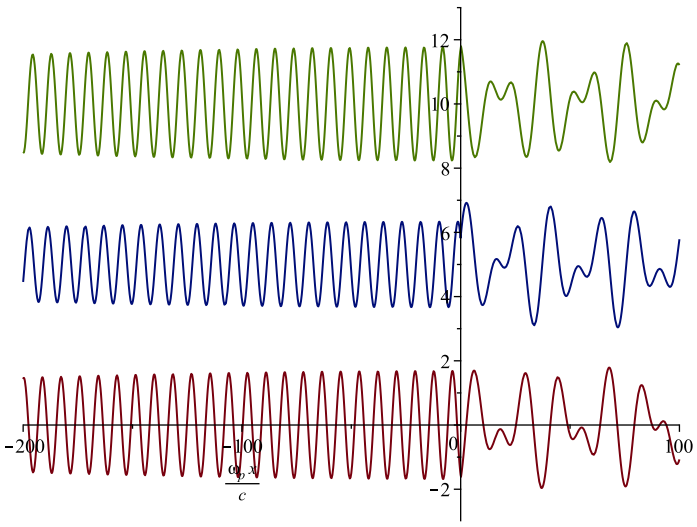

Figure 11. H field at the interface between the vacuum ($x < 0$) and the metamaterial with negative index of refraction ($x > 0$) from the bottom to the top for $\omega_p t$ ranging from 5 to 9 in the steps of 2.

5. Oblique Incidence on a Metamaterial: A Positive to Negative Index Refraction

Consider the 2D motion of the H-polarized field given by $\mathbf{H} = [0, 0, H_z]^T$ and $\mathbf{E} = [E_x, E_y, 0]^T$. In the vacuum, the third component of the incident H field is given by

$$H_z^{in} = B_0 e^{i(k\hat{\kappa}_i \cdot \mathbf{x} - kct)}, \tag{30}$$

where k is the wave number in vacuum ($x < 0$), $\mathbf{x} = (x, y)$, the incident wave propagation direction $\hat{\kappa}_i = (\cos\theta_i, \sin\theta_i)$ and θ_i is the angle of incidence between the incident wave and the normal vector $\hat{n} = (1, 0, 0)$ of the interface ($x = 0$). After the incident wave hits the interface ($x = 0$), the reflected wave has the form of

$$H_z^{re} = -\mathcal{R}(ck) B_0 e^{i(k\hat{\kappa}_r \cdot \mathbf{x} - kct)}, \tag{31}$$

where $\mathcal{R}(ck)$ is the reflection coefficient, the reflected wave propagation direction $\hat{\kappa_r} = (-\cos\theta_r, \sin\theta_r)$ and $\theta_r = \theta_i$ is the reflective angle between the reflective wave and the interface normal.

In the negative index metamaterial ($x > 0$), the transmitted wave has the form of

$$H_z^{tr} = \mathcal{T}(ck)\frac{B_0}{\mu_{eff}(ck)}e^{i(k_m\hat{\kappa_t}\cdot\mathbf{x}-kct)}, \tag{32}$$

where $\mathcal{T}(ck)$ is the transmission coefficient, k_m is the wave number in the media, the propagation direction in the effective media $\hat{\kappa_t} = (\cos\theta_t, \sin\theta_t)$, θ_t is the refractive angle between the refractive wave and the interface normal and by the Snell's Law $\sin\theta_i = n_{eff}\sin\theta_t$.

From the Maxwell equation, at the interface ($x = 0$), we have the transmission conditions

$$[\hat{n} \times \mathbf{H}] = 0 \text{ at } x = 0 \tag{33}$$

and

$$[\hat{n} \times \mathbf{E}] = 0 \text{ at } x = 0. \tag{34}$$

The transmission condition (33) shows

$$H_z^{in} + H_z^{re} = H_3^{tr} \text{ at } x = 0 \tag{35}$$

which implies that

$$B_0 e^{i(k\hat{\kappa_i}\cdot\mathbf{x}-kct)} - \mathcal{R}(ck)B_0 e^{i(k\hat{\kappa_r}\cdot\mathbf{x}-kct)} = \mathcal{T}(ck)\frac{B_0}{\mu_{eff}(ck)}e^{i(k_m\hat{\kappa_t}\cdot\mathbf{x}-kct)} \text{ at } x = 0. \tag{36}$$

Since $k\sin\theta_i = k_m\sin\theta_t$ by Snell's Law, (36) becomes

$$1 - \mathcal{R}(ck) = \frac{\mathcal{T}(ck)}{\mu_{eff}(ck)}. \tag{37}$$

We also have

$$\mathbf{E} = \frac{1}{i\omega\epsilon(\mathbf{x})}\nabla \times \mathbf{H}. \tag{38}$$

So the transmission condition (34) shows

$$[\epsilon^{-1}(\mathbf{x})\partial_x H_z]\Big|_{x=0} = 0. \tag{39}$$

Here

$$\epsilon(\mathbf{x}) = \begin{cases} 1 & x < 0, \\ \epsilon_{eff}(ck) & x > 0. \end{cases}$$

Then we have

$$\partial_x(H_z^{in} + H_z^{re})\Big|_{x=0} = \epsilon_{eff}^{-1}\,\partial_x H_z^{tr}\Big|_{x_1=0} \tag{40}$$

which implies

$$(1+\mathcal{R}(ck))\,k\cos\theta_i = \frac{\mathcal{T}(ck)\epsilon_{eff}^{-1}(ck)}{\mu_{eff}(ck)}k_m\cos\theta_t. \tag{41}$$

The linear system (37) and (41) has the solution

$$\mathcal{R}(ck) = \frac{\frac{k_m}{k}\cos\theta_t - \epsilon_{eff}\cos\theta_i}{\frac{k_m}{k}\cos\theta_t + \epsilon_{eff}\cos\theta_i} \tag{42}$$

and

$$\mathcal{T}(ck) = \frac{2\mu_{eff}(ck)\epsilon_{eff}\cos\theta_i}{\frac{k_m}{k}\cos\theta_t + \epsilon_{eff}\cos\theta_i} \tag{43}$$

Collecting results we have

Proposition 2. Waveforms in vacuum and effective material in 2D. *The $\hat{z}$ component of the H field is the only non zero component of the H field wave form in vacuum ($x<0$) and is*

$$H_{vac}(k_0,\mathbf{x},t) \;=\; \int_{-\infty}^{\infty} A(k)B_0[e^{i(k\hat{\kappa}_i\cdot\mathbf{x}-kct)} - \mathcal{R}(ck)e^{i(k\hat{\kappa}_r\cdot\mathbf{x}-kct)}]\,dk. \tag{44}$$

The $\hat{z}$ component of the H field is the only non zero component of the H field wave form in the metamaterial ($x>0$) and is

$$H_{eff}(k_0,\mathbf{x},t) \;=\; \int_{-\infty}^{\infty} A(k)\mathcal{T}(ck)\frac{B_0}{\mu_{eff}(ck)}e^{i(k_m\hat{\kappa}_t\cdot\mathbf{x}-kct)}\,dk. \tag{45}$$

Here $H_{vac}(k_0,\mathbf{x},t) = H_{eff}(k_0,\mathbf{x},t)$ at the interface $x_1=0$, and

$$\mathcal{R}(ck) = \frac{\frac{k_m}{k}\cos\theta_t - \epsilon_{eff}\cos\theta_i}{\frac{k_m}{k}\cos\theta_t + \epsilon_{eff}\cos\theta_i} \tag{46}$$

and

$$\mathcal{T}(ck) = \frac{2\mu_{eff}(ck)\epsilon_{eff}\cos\theta_i}{\frac{k_m}{k}\cos\theta_t + \epsilon_{eff}\cos\theta_i}.$$

We consider the signal composed of waves inside a frequency band for which $A(k)$ is defined by (23). The transmitted signal (45) can be written as

$$\begin{aligned} H_{eff} \;=\; & \frac{\omega_p a}{c}\frac{1}{\sqrt{2\pi}}\int_{-\infty}^{\infty} e^{-\frac{(\frac{\omega}{\omega_p}-\frac{\bar{\omega}}{\omega_p})^2(\frac{\omega_p a}{c})^2}{2}}\hat{\chi}(\omega/\omega_p)\times \\ & \frac{B_0\mathcal{T}(\omega/\omega_p)}{\mu_{eff}(\omega/\omega_p)}e^{i[(n_{eff}\frac{\omega}{\omega_p})(\frac{\omega_p x_1}{c}\cos\theta_t+\frac{\omega_p x_2}{c}\sin\theta_t)-(\frac{\omega}{\omega_p})(\omega_p t)]}\,d(\tfrac{\omega}{\omega_p}) \end{aligned} \tag{47}$$

Similarly the signal in the vacuum can be rewritten as

$$\begin{aligned} H_{vac} \;=\; & \frac{\omega_p a}{c}\frac{1}{\sqrt{2\pi}}\int_{-\infty}^{\infty} e^{-\frac{(\frac{\omega}{\omega_p}-\frac{\bar{\omega}}{\omega_p})^2(\frac{\omega_p a}{c})^2}{2}}\hat{\chi}(\omega/\omega_p)B_0\times \\ & [e^{i[(\frac{\omega}{\omega_p})(\frac{\omega_p x_1}{c}\cos\theta_i+\frac{\omega_p x_1}{c}\sin\theta_i)-(\frac{\omega}{\omega_p})(\omega_p t)]} \\ & -\mathcal{R}(\omega/\omega_p)e^{i[(\frac{\omega}{\omega_p})(-\frac{\omega_p x_1}{c}\cos\theta_i+\frac{\omega_p x_2}{c}\sin\theta_i)-(\frac{\omega}{\omega_p})(\omega_p t)]}]\,d(\tfrac{\omega}{\omega_p}). \end{aligned} \tag{48}$$

In this example, we take as before $\frac{\omega_p a}{c} = 300$, $\omega_L/\omega_p = 0.735$ and $\omega_U/\omega_p = 0.74$. Let the dimensionless center frequency be $\frac{\bar{\omega}}{\omega_p} = 0.7375$ and the incident angle $\theta_i = 16^\circ$. We use a Riemann sum and approximate the integrals by the sum of two rectangles. So

$$\begin{aligned} H_{eff} &= \frac{\omega_p a}{c}\frac{1}{\sqrt{2\pi}}\int_{-\infty}^{\infty}\hat{\chi}(\omega/\omega_p)B_0\hat{F}(\omega/\omega_p)\,d(\frac{\omega}{\omega_p}) \\ &= \frac{\omega_p a}{c}\frac{1}{\sqrt{2\pi}}\int_{0.735}^{0.74}B_0\hat{F}(\omega/\omega_p)\,d(\frac{\omega}{\omega_p}) \\ &\approx \frac{\omega_p a}{c}\frac{1}{\sqrt{2\pi}}\Delta(\frac{\omega}{\omega_p})B_0[\hat{F}(0.735)+\hat{F}(0.74)], \end{aligned} \tag{49}$$

where $\hat{F} = e^{-\frac{(\frac{\omega}{\omega_p}-\frac{\bar{\omega}}{\omega_p})^2(\frac{\omega_p a}{c})^2}{2}}\frac{\mathcal{T}(\omega/\omega_p)}{\mu_{eff}(\omega/\omega_p)}e^{i[(n_{eff}\frac{\omega}{\omega_p})(\frac{\omega_p x_1}{c}\cos\theta_t+\frac{\omega_p x_2}{c}\sin\theta_t)-(\frac{\omega}{\omega_p})(\omega_p t)]}$ and $\frac{\omega_p a}{c}\frac{1}{\sqrt{2\pi}}\Delta(\frac{\omega}{\omega_p})B_0$ is a constant. Notice that $\theta_t = \arcsin(\mathbf{n}_{eff}\sin\theta_i)$. Therefore, $\theta_t = -24.12^\circ$ when $\frac{\omega}{\omega_p} = 0.735$ and $\theta_t = -39.20^\circ$ when $\frac{\omega}{\omega_p} = 0.74$. And

$$\begin{aligned} H_{vac} &= \frac{\omega_p a}{c}\frac{1}{\sqrt{2\pi}}\int_{-\infty}^{\infty}\hat{\chi}(\omega/\omega_p)B_0\hat{G}(\omega/\omega_p)\,d(\frac{\omega}{\omega_p}) \\ &= \frac{\omega_p a}{c}\frac{1}{\sqrt{2\pi}}\int_{0.735}^{0.74}B_0\hat{G}(\omega/\omega_p)\,d(\frac{\omega}{\omega_p}) \\ &\approx \frac{\omega_p a}{c}\frac{1}{\sqrt{2\pi}}\Delta(\frac{\omega}{\omega_p})B_0[\hat{G}(0.735)+\hat{G}(0.74)], \end{aligned} \tag{50}$$

where

$$\begin{aligned} \hat{G} = e^{-\frac{(\frac{\omega}{\omega_p}-\frac{\bar{\omega}}{\omega_p})^2(\frac{\omega_p a}{c})^2}{2}}[&e^{i[(\frac{\omega}{\omega_p})(\frac{\omega_p x_1}{c}\cos\theta_i+\frac{\omega_p x_1}{c}\sin\theta_i)-(\frac{\omega}{\omega_p})(\omega_p t)]} \\ &-\mathcal{R}(\omega/\omega_p)e^{i[(\frac{\omega}{\omega_p})(-\frac{\omega_p x_1}{c}\cos\theta_i+\frac{\omega_p x_2}{c}\sin\theta_i)-(\frac{\omega}{\omega_p})(\omega_p t)]}]. \end{aligned}$$

Figure 12 shows the contour map of H field at the interface between the vacuum ($x < 0$) and the effective double negative material ($x > 0$).

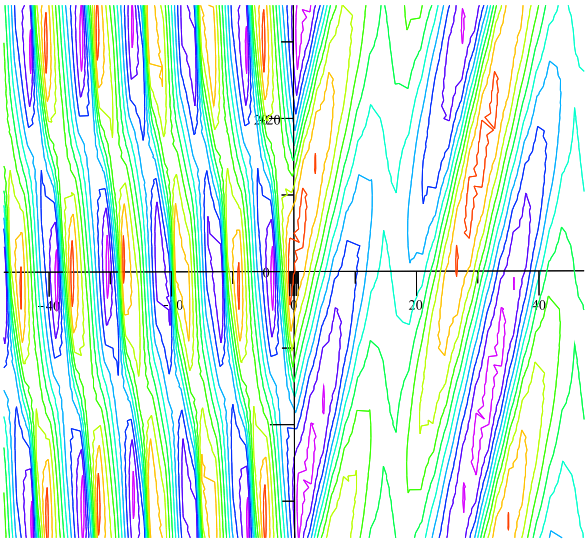

Figure 12. Contour map of H field with the incident angle $\theta_i = 16^\circ$ at the interface between the vacuum ($x < 0$) and effective double negative material ($x > 0$) when $\omega_p t = 0$.

Now consider another signal but with with $\omega_L/\omega_p = 0.95$ and $\omega_U/\omega_p = 0.96$. The paper [36] shows that when the dimensionless frequency $\frac{\omega}{\omega_p}$ lies in the interval $[0.95, 0.96]$, the effective permittivity and effective permeability of the material are simultaneously positive. Let the dimensionless center frequency $\frac{\bar{\omega}}{\omega_p} = 0.955$ and the incident angle $\theta_i = 16^\circ$. Note that the refractive angle $\theta_t = 75.57^\circ$ when $\frac{\omega}{\omega_p} = 0.95$ and $\theta_t = 55.00^\circ$ when $\frac{\omega}{\omega_p} = 0.96$. Figure 13 gives the contour map of H field at the interface between the vacuum ($x < 0$) and the effective double positive material ($x > 0$).

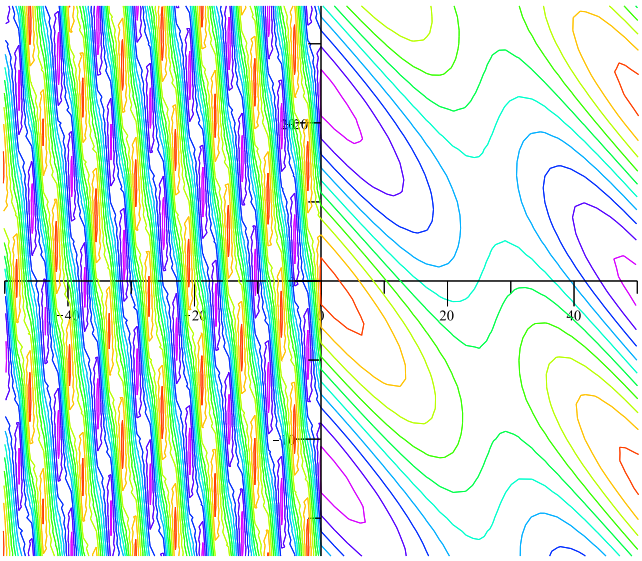

Figure 13. Contour map of H field with the incident angle $\theta_i = 16^\circ$ at the interface between the vacuum ($x < 0$) and effective double positive material ($x > 0$) when $\omega_p t = 0$.

6. Conclusions

We have considered the refraction of incoming signals traveling from free space into a metamaterial. The metamaterial considered in this paper is made up of a periodic sub-wavelength array of non-magnetic resonators. We show that the resonator geometry influences the direction of the transmitted signal depending on the signal's center frequency and bandwidth. Here the directionality of the refracted signal and its frequency dependence is explicitly controlled by sub-wavelength resonances that can be controlled by adjusting the geometry of the sub-wavelength scatters. We present the time domain representation for the refracted signals and use this representation in the numerical simulation of their behavior. The simulation shows that the medium can be designed to simultaneously refract signals both positively or negatively depending on the signal's center frequency and band width.

Author Contributions: Conceptualization, Y.C. and R.L.; methodology, Y.C. and R.L.; software, Y.C.; validation, Y.C. and R.L.; writing—original draft preparation, Y.C. and R.L.; writing—review and editing, Y.C. and R.L.; funding acquisition, R.L.

Funding: This research was funded by NSF Grant DMS-1813698.

Conflicts of Interest: The authors declare no conflict of interest. The funders had no role in the design of the study; in the collection, analyses, or interpretation of data; in the writing of the manuscript, or in the decision to publish the results.

References

1. Bohren, C.F.; Huffman, D.H. *Absorption and Scattering of Light by Small Particles*; Wiley: Hoboken, NJ, USA, 2004.
2. Pendry, J.; Holden, A.; Robbins, D.; Stewart, W. Magnetisim from conductors and enhanced nonlinear phenomena. *IEEE Trans. Microw. Theory Tech.* **1999**, *47*, 2075–2084. [CrossRef]

3. Pendry, J.; Holden, A.; Robbins, D.; Stewart, W. Low frequency plasmons in thin-wire structures. *J. Phys. Condens. Matter.* **1998**, *10*, 4785–4809. [CrossRef]
4. Smith, D.R.; Padilla, W.; Vier, D.; Nemat-Nasser, S.; Schultz, S. Composite medium with simultaneously negative permeability and permittivity. *Phys. Rev. Lett.* **2000**, *84*, 4184–4187. [CrossRef] [PubMed]
5. Shelby, R.A.; Smith, D.R.; Schultz, S. Experimental verification of a negative index of refraction. *Science* **2001**, *292*, 77–79. [CrossRef] [PubMed]
6. Ziolkowski, R.W. Pulsed and CW Gaussian beam interactions with double negative metamaterial slabs. *Opt. Express* **2003**, *11*, 662–681. [CrossRef] [PubMed]
7. Babych, N.O.; Kamotski, I.V.; Smyshlyaev, V.P. Homogenization of spectral problems in bounded domains with doubly high contrast. *Netw. Heterog. Med.* **2008**, *3*, 413–436.
8. Bouchitté, G.; Schweizer, B. Homogenization of Maxwell's equations in a split ring geometry. *Multiscale Model. Simul.* **2010**, *8*, 717–750. [CrossRef]
9. Bouchitté, G.; Felbacq, D. Homogenization near resonances and artificial magnetism from dielectrics. *C. R. Math.* **2004**, *339*, 377–382. [CrossRef]
10. Dolling, G.; Enrich, C.; Wegener, M.; Soukoulis, C.M.; Linden, S. Low-loss negative-index metamaterial at telecommunication wavelengths. *Opt. Lett.* **2006**, *31*, 1800–1802. [CrossRef] [PubMed]
11. Fortes, S.P.; Lipton, R.P.; Shipman, S.P. Convergent power series for fields in positive or negative high-contrast periodic media. *Commun. Part. Differ. Equat.* **2011**, *36*, 1016–1043. [CrossRef]
12. Huangfu, J.; Ran, L.; Chen, H.; Zhang, X.; Chen, K.; Grzegorczyk, T.M.; Kong, J.A. Experimental confirmation of negative refractive index of a metamaterial composed of Ω-like metallic patterns. *Appl. Phys. Lett.* **2004**, *84*, 1537. [CrossRef]
13. Kohn, R.; Shipman, S. Magnetism and homogenization of micro- resonators. *Multiscale Model. Simul.* **2008**, *7*, 62–92. [CrossRef]
14. Lipton, R.; Polizzi, A.; Thakur, L. Novel metamaterial surfaces from perfectly conducting subwavelength corrugations. *SIAM J. Appl. Math.* **2017**, *77*, 1269–1291.
15. Lipton, R.; Schweizer, B. Effective Maxwell's equations for perfectly conducting split ring resonators. *Arch. Ration. Mech. Anal.* **2018**, *229*, 1197–1221. [CrossRef]
16. Shalaev, V.M.; Cai, W.; Chettiar, U.K.; Yuan, H.K.; Sarychev, A.K.; Drachev, V.P.; Kildishev, A.V. Negative index of refraction in optical metamaterials. *Opt. Lett.* **2005**, *30*, 3356–3358. [CrossRef] [PubMed]
17. Zhang, F.; Potet, S.; Carbonell, J.; Lheurette, E.; Vanbesien, O.; Zhao, X.; Lippens, D. Negative-zero-positive refractive index in a prism-like omega-type metamaterial. *IEEE Trans. Microw. Theory Tech.* **2008**, *56*, 2566–2573. [CrossRef]
18. Zhang, S.; Fan, W.; Minhas, B.K.; Frauenglass, A.; Malloy, K.J.; Brueck, S.R.J. Midinfrared resonant magnetic nanostructures exhibiting a negative permeability. *Phys. Rev. Lett.* **2005**, *94*, 037402. [CrossRef] [PubMed]
19. Zhikov, V.V. On an extension of the method of two-scale convergence and its applications. *Sb. Math.* **2000**, *191*, 973–1014. [CrossRef]
20. Zhou, X.; Zhao, X.P. Resonant condition of unitary dendritic structure with overlapping negative permittivity and permeability. *Appl. Phys. Lett.* **2007**, *91*, 181908. [CrossRef]
21. Wheeler, M.S.; Aitchison, J.S.; Mojahedi, M. Coated non-magnetic spheres with a negative index of refraction at infrared frequencies. *Phys. Rev. B* **2006**, *73*, 045105. [CrossRef]
22. Yannopapas, V. Negative refractive index in the near-UV from Au-coated CuCl nanoparticle superlattices. *Phys. Status Solidi (RRL)* **2007**, *1*, 208–210. [CrossRef]
23. Yannopapas, V. Artificial magnetism and negative refractive index in three-dimensional metamaterials of spherical particles at near-infrared and visible frequencies. *Appl. Phys. A* **2007**, *87*, 259–264. [CrossRef]
24. Huang, K.C.; Povinelli, M.L.; Joannopoulos, J.D. Negative effective permeability in polaritonic photonic crystals. *Appl. Phys. Lett.* **2004**, *85*, 543.
25. Peng, L.; Ran, L.; Chen, H.; Zhang, H.; Kong, L.A.; Grzegorczyk, T.M. Experimental observation of left-handed behavior in an array of standard dielectric resonators. *Phys. Rev. Lett.* **2007**, *98*, 157403. [CrossRef] [PubMed]
26. Vynck, K.; Felbacq, D.; Centeno, E.; Cabuz, A.I.; Cassagne, D.; Guizal, B. All-dielectric rod-type metamaterials at optical frequencies. *Phys. Rev. Lett.* **2009**, *102*, 133901. [CrossRef] [PubMed]
27. Alu, A.; Engheta, N. Dynamical theory of artifical optical magnetism produced by rings of plasmonic nanoparticles. *Phys. Rev. B* **2008**, *78*, 085112. [CrossRef]

28. Shvets, G.; Urzhumov, Y. Engineering the electromagnetic properties of periodic nanostructures using electrostatic resonances. *Phys. Rev. Lett.* **2004**, *93*, 243902. [CrossRef] [PubMed]
29. Service, R.F. Next Wave of metamaterials hopes to fuel the revolution. *Science* **2010**, *327*, 138–139. [CrossRef] [PubMed]
30. Shalaev, V. Optical negative-index metamaterials. *Nat. Photonics* **2007**, *1*, 41–48. [CrossRef]
31. Fujii, G.; Matsumoto, T.; Takahashi, T.; Ueta, T. A study on the effect of filling factor for laser action in dielectric random media. *Appl. Phys. A* **2012**, *107*, 33–42. [CrossRef]
32. Fujii, G.; Matsumoto, T.; Takahashi, T.; Ueta, T. Study on transition from photonic-crystal laser to random laser. *Opt. Express* **2012**, *20*, 7300–7315. [CrossRef] [PubMed]
33. Wiersma, D.S. Disordered photonics. *Nat. Photonics* **2013**, *7*, 188–196. [CrossRef]
34. Chen, Y.; Lipton, R. Resonance and double negative behavior in metamaterials. *Arch. Ration. Mech. Anal.* **2013**, *209*, 835–868. [CrossRef]
35. Chen, Y.; Lipton, R. Tunable double negative band structure from non-magnetic coated rods. *New J. Phys.* **2010**, *12*, 083010. [CrossRef]
36. Chen, Y.; Lipton, R. Double Negative Dispersion Relations from Coated Plasmonic Rods. *Multiscale Model. Simul.* **2013**, *11*, 192–212. [CrossRef]
37. Chen, Y.; Lipton, R. Multiscale methods for engineering double negative metamaterials. *Photonics Nanostruct. Fundam. Appl.* **2013**, *11*, 442–452. [CrossRef]
38. Bergman, D.J. The dielectric constant of a simple cubic array of identical spheres. *J. Phys. C Solid State Phys.* **1979**, *12*, 4947–4960. [CrossRef]
39. McPhedran, R.C.; Milton, G.W. Bounds and exact theories for the transport properties of inhomogeneous media. *Appl. Phys. A* **1981**, *26*, 207–220. [CrossRef]